

Autler-Townes Effects in Attosecond Circular Polarization Molecular Photoionization

Kai-Jun Yuan¹, Zhigang Sun^{2,3}, and André D Bandrauk¹

¹ Laboratoire de Chimie Théorique, Faculté des Sciences, Université de Sherbrooke, Sherbrooke, Québec, Canada, J1K 2R1

² Center for Theoretical and Computational Chemistry and State Key Laboratory of Molecular Reaction Dynamics, Dalian Institute of Chemical Physics, Chinese Academy of Sciences, Dalian 116023, P.R. China

³ Synergetic Innovation Center of Quantum Information and Quantum Physics, University of Science and Technology of China, Hefei, Anhui 230026, P.R. China

E-mail: kaijun.yuan@usherbrooke.ca; zsun@dicp.ac.cn; andre.bandrauk@usherbrooke.ca

Abstract. We present molecular photoionization simulations by intense ($I \sim 10^{16}$ W/cm²) few cycle circularly polarized *attosecond* extreme ultraviolet laser pulses for aligned H₂⁺ from numerical solutions of the corresponding time-dependent Schrodinger equation. With appropriate laser pulse parameters, circular attosecond coherent electron wave packets (CEWPs) are created in excited Rydberg states. Such CEWPs are spatially localized during ionization processes, thus resulting in sufficient population oscillations between the resonant excited Rydberg states and the initial ground state. Consequently Autler-Townes splitting in circular polarization energy spectra is predicted, which is shown to be critically sensitive to the pulse intensity, duration, and polarization. The resulting photoelectron angular distributions are rotated with respect to the molecular axis due to the nonspherical Coulomb potential of the molecule, resulting in different ionization rates at different laser polarization-molecular angles.

1. Introduction

Rapid developments in advanced laser pulse technology [1, 2] provide the tools necessary for investigating electron dynamics on the attosecond (1 asec=10⁻¹⁸ s) time scale and in the nonlinear nonperturbative regime. Such ultrashort laser pulses offer now the possibility of creating coherent electron wave packets (CEWPs) inside atoms and molecules on the attosecond time scale and sub-nanometer dimension [3-5]. Recently attosecond extreme ultraviolet (XUV) light from high-order harmonics (HHG) and free electron lasers (FEL), or combined with infrared (IR) laser pulses has been used to monitor electron dynamics in CEWPs by measuring photoelectron angular and energy distributions thus revealing effects of atomic and molecular orbital configurations [6], multi-pathway quantum interference [7-11] and electron correlations [13, 14]. XUV-pump-XUV-probe experiments have been adopted in molecular isomerization in acetylene cations [15]. It has also been shown that due to ac Stark effects in the continuum, dynamic interference of the photoelectrons emitted at different time can be observed with high frequency laser pulses [16]. These new experiments are done mainly with ultrashort intense *linearly* polarized pulses. Ultrashort circularly polarized laser pulses offer new avenues to investigate electron dynamics on attosecond time scales [17-21]. We have recently proposed



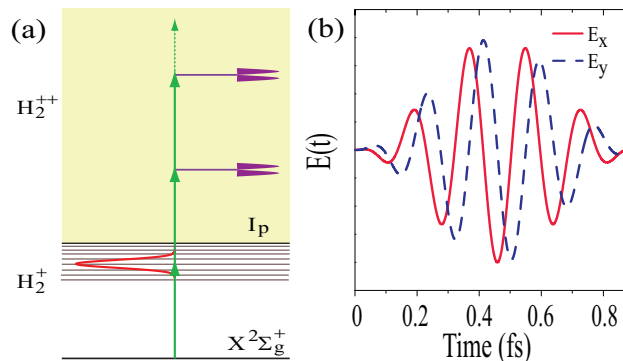


Figure 1. (Color online) (a) Schematic illustrations of multiphoton ionization pathways from the $H_2^+ X^2\Sigma_g^+$ electron state at $R_e = 2$ a.u. in (b) intense five cycles circularly polarized FWHM=460 asec at $\lambda = 55$ nm ($\omega = 0.828$ a.u., $\tau = 184$ asec) XUV laser fields $E(t)$.

methods of generating *circularly* polarized attosecond pulses from circularly polarized molecular HHG [22, 23] using the nonspherical symmetry of molecules which allows for generating circularly polarized harmonics. Circularly polarized laser pulses have also been shown to be important to induce perturbatively circular electron ring currents in cyclic molecules, thus producing intense internal magnetic fields [24, 25] and to investigate recollision of electrons in double ionization [19, 20]. In [21], two color counter-propagating circularly polarized laser pulses are studied to study the scaling of the maximum HHG spectrum and stabilization at high frequency in [26]. We have recently proposed that with intense few cycle circularly polarized XUV pulses, strong attosecond magnetic field pulses with several tens of Teslas can be induced in molecules [27], thus suggesting a new experimental tool for nonlinear magneto-optics.

In this work we study photoionization of the single electron aligned H_2^+ with these new intense circularly polarized attosecond XUV laser pulses, as schematically illustrated in figure 1. It is found that with proper conditions of the driving laser pulse, Autler-Townes (AT) splitting can be observed in molecular photoelectron energy distributions from localized circular CEWPs. AT splitting was first observed in radio-frequency transitions in atoms [28], which resulted from Rabi oscillations of the population between two specified atomic states. Molecular AT splitting resulting from vibrational coherent states with ultrashort femtosecond laser pulses has also been predicted in molecular ionization [29, 30]. Effects of molecular orientation and rotation on such splitting were also investigated [31]. To the best of our knowledge such observations of AT doublets resulting from coherent localized electronic wave packets have not been reported in photoionization due to the rapid electron motion on its natural time scale, the attosecond. A spatially localized electronic wave packet is difficult to confine and measure with linearly polarized laser pulses of moderate intensity and femtosecond (1fs= 10^{-15} s) duration. Circularly polarized laser pulses differ from linear polarization by having a constant rotating electric field. We show that circularly polarized attosecond XUV laser pulses produce “spinning” electrons, and the excited circular CEWPs can be localized on the sub-nanometer molecular dimension scale. Consequently, AT doublets are shown to occur in molecular ionization energy-resolved photoelectron angular distributions (MPADs) with pulse intensities near 10^{16} W/cm². Circularly polarized attosecond laser pulses are shown to be essential in observing new coherence effects in circular CEWPs, thus offering the possibility to observe AT splittings at high intensities due to circular polarization Rabi oscillations. The proposal of generating circularly polarized attosecond pulses [22, 23] make it thus possible to create spinning and localized circular electron wave packets in matter on attosecond time scale.

The paper is arranged as follows: In section 2, we briefly describe the computational methods

for time-dependent quantum electron wave packets obtained from the corresponding time-dependent Schrödinger equation (TDSE). The numerical results of photoelectron energy spectra by intense ultrashort few cycle circularly polarized UV pulses for H_2^+ are presented in section 3. Effects of the pulse intensity, duration, wavelength, and polarization on the AT splitting doublets are investigated. Finally, we summarize our findings in section 4. Throughout this paper, atomic units (a.u.) $e = \hbar = m_e = 1$ are used, for which the a.u. of intensity $I_0 = 3.51 \times 10^{16} \text{ W/cm}^2$ and corresponding electric field $E_0 = 5 \times 10^9 \text{ V/cm}$.

2. Numerical methods

Simulations are performed on an aligned molecular ion H_2^+ by solving numerically the corresponding TDSEs [32, 33] within a static (Born-Oppenheimer approximation, BOA) nuclear frame,

$$i \frac{\partial}{\partial t} \psi(\mathbf{r}, t) = [H_0 + V_L(\mathbf{r})] \psi(\mathbf{r}, t), \quad (1)$$

where H_0 is the field free molecular Hamiltonian and $V_L(\mathbf{r})$ the interaction term. An intense few cycle circularly polarized attosecond XUV laser pulses with wavelength $\lambda = 55 \text{ nm}$ (angular frequency $\omega = 2\pi c/\lambda = 0.828 \text{ a.u.}$) is used to ionize the molecular ion H_2^+ . We use a three dimensional (3D) model with static nuclei, enabling to go beyond perturbation theory and independent of gauge transformations [34, 35]. Such a fixed nuclei approach ignoring the vibrational and rotational degrees of freedom is appropriate due to the longer femtosecond/picosecond time scale of nuclear (vibrational/rotational) motions since the vibrational period of ground state H_2^+ is $\sim 15 \text{ fs}$. The 3D TDSE is solved using cylindrical coordinates (ρ, θ, z) with the molecular plane $x = \rho \cos \theta$ and $y = \rho \sin \theta$. The molecular Hamiltonian is expressed as

$$H_0(\rho, \theta, z) = -\frac{1}{2\rho} \frac{\partial}{\partial \rho} \left(\rho \frac{\partial}{\partial \rho} \right) - \frac{1}{2\rho^2} \frac{\partial^2}{\partial \theta^2} - \frac{1}{2} \frac{\partial^2}{\partial z^2} + V(\rho, \theta, z), \quad (2)$$

where $V(\rho, \theta, z)$ is the two center electron-nuclear potential. The molecule ion is aligned along the x axis during ionization, which can be readily achieved with orientational laser technology [36]. The laser-electron radiative coupling is described by

$$V_L(\rho, \theta, t) = \mathbf{r} \cdot \mathbf{E}(t) = \rho \cos \theta E_x(t) + \rho \sin \theta E_y(t) \quad (3)$$

in the length gauge for circularly polarized laser pulses with forms,

$$\mathbf{E}(t) = E f(t) [\mathbf{e}_x \cos(\omega t) + \mathbf{e}_y \sin(\omega t)], \quad (4)$$

where $\hat{e}_{x/y}$ are the polarization directions. Such a field induces electric currents in the ring molecular (x, y) plane. For linear polarization, $E_y(t) = 0$ with the field parallel to the molecular x axis. A smooth $\sin^2(\pi t/n\tau)$ pulse envelope with maximum amplitude E for intensity $I = I_x = I_y = \frac{1}{2} c \varepsilon_0 E^2$ is adopted, where one optical cycle $\tau = 2\pi/\omega$. The laser electric field $\int E(t) dt = 0$ satisfies Maxwell's equation in the propagation region to mimic the electric field of the electromagnetic wave [1].

We numerically solve the 3D TDSE by a second order split operator method in the time step δt combined with a fifth order finite difference method and Fourier transform technique in the spatial steps $\delta \rho$, δz , and $\delta \theta$ [37, 38]. The time step is taken to be $\delta t = 0.01 \text{ a.u.} = 0.24 \text{ asec}$. The spatial discretization is $\delta \rho = \delta z = 0.25 \text{ a.u.}$ for a radial grid range $0 \leq \rho \leq 128 \text{ a.u.}$ and $|z| \leq 64 \text{ a.u.}$, and the angle grid size $\delta \theta = 0.025 \text{ radian}$. The spatial grid step ensures

the description of a maximum momentum $\Delta p_e = \pi/\Delta\rho \approx 13$ a.u. and energy $E_e = \Delta p_e^2/2 = 80$ a.u. for the photoelectron spectrum. To prevent unphysical effects due to the reflection of the wave packet from the boundary, we multiply $\psi(\rho, \theta, z, t)$ by a “mask function” or absorber in the radial coordinate with the form $\cos^{1/8}[\pi(\rho - \rho_a)/2\rho_{\text{abs}}]$. For all results reported here we set the absorber domain $\rho_a = \rho_{\text{max}} - \rho_{\text{abs}} = 104$ a.u. with $\rho_{\text{abs}} = 24$ a.u., exceeding well the field induced electron oscillation $\alpha_d = E/\omega^2$ of the electron.

For an intense laser pulse, a quite large grid range must be used to obtain via Fourier transform the high energy of the ejected electron in the ionization spectra. In the present work we use an efficient method by calculating a radial flux (electron current density) $\mathcal{J}(t)$ to describe the ionization spectra, where the high kinetic energy of the free electron can be accurately calculated. At an asymptotic point $\rho_0 = 100$ a.u., the electron wave function $\psi(\mathbf{r}, t)$ generates the flux $\mathcal{J}(t)$ in the molecular and laser polarization (x, y) plane before the grid absorption at boundary. For attosecond photoionization processes, the laser duration is very short. At such large asymptotic point ρ_0 , the angular flux distributions can be ignored, i.e., $1/\rho_0 \partial/\partial\theta|_{\rho_0} \hat{e}_\theta \ll \partial/\partial\rho|_{\rho_0} \hat{e}_\rho$. As a result we only need to consider the radial part of the electronic flux along the radial direction, $\partial/\partial\rho|_{\rho_f} \hat{e}_\rho$. The time-independent energy-resolved angular differential yield (photoelectron spectra) is obtained by a Fourier transform:

$$\begin{aligned}\psi(\theta, E_e)|_{\rho_0} &= \int_{t_p}^{t_f} \psi(\theta, t)|_{\rho_0} e^{iE_e t} dt, \\ \psi'(\theta, E_e)|_{\rho_0} &= \int_{t_p}^{t_f} \frac{\partial\psi(\theta, t)}{\partial\rho}|_{\rho_0} e^{iE_e t} dt, \\ \mathcal{J}(\theta, E_e) &\sim \text{Re} \left[\frac{1}{2i} \psi'^*(\theta, E_e)|_{\rho_0} \psi(\theta, E_e)|_{\rho_0} \right],\end{aligned}\tag{5}$$

where t_p is time after pulses switch off and $t_f = 80\tau$ to insure that the photoelectrons pass through the asymptotic point ρ_0 . $E_e = p_e^2/2$ (in a.u.) is the kinetic energy of a free electron with wave vector $k = p_e = 2\pi/\lambda_e$ (in a.u.), $p_e = (p_x^2 + p_y^2)^{1/2}$ is the momentum of a photoelectron of wavelength λ_e . With the transformation $p_x = p_e \cos\theta$ and $p_y = p_e \sin\theta$, we then obtain the two dimensional momentum distributions of photoelectrons from equation (5).

3. Results and discussions

The excitation process and the laser pulse are illustrated in figure 1. The laser wavelength is chosen at $\lambda = 55$ nm (angular frequency $\omega = 0.828$ a.u., 1 optical cycle $\tau = 184$ asec), slightly below the equilibrium, $R_e = 2$ a.u., ionization potential $I_p = 1.1$ a.u., thus ensuring at least a two photon absorption to ionize H_2^+ . Because the lifetimes of Rydberg states are significantly longer than the attosecond XUV pulse duration, population then can be transferred from the ground $X^2\Sigma_g^+$ state to the Rydberg states after absorption of one photon, then returning to the ground state. Thus Rabi oscillations will occur between these states coupled strongly by a one photon transition, resulting in an AT splitting, figure 1, producing doublets in the MPAD. The full width at half maximum (FWHM) of the XUV laser pulse is always fixed at 460 asec (5 cycles). Four different pulse intensities $I = 1 \times 10^{15}$ W/cm² ($E = 0.169$ a.u.), 5×10^{15} W/cm² (0.377 a.u.), 1×10^{16} W/cm² (0.534 a.u.), and 2×10^{16} W/cm² (0.755 a.u.) are used to ionize H_2^+ , respectively. With such strong intensity pulses, the Keldysh parameter $\gamma = \sqrt{I_p/2U_p} \geq 2.3$ used to characterize strong field physics, where $U_p = I/4\omega$ is the ponderomotive energy, implies a multi-photon regime [1].

We show in figure 2 the angular distributions $\mathcal{J}(\theta, E_e)$ in the H_2^+ ground $X^2\Sigma_g^+$ state induced with five cycle circularly polarized attosecond XUV laser pulses. Only the distributions with energies $E_e < 1.9$ a.u. are reported, i.e., two and three photon ionization photoelectron spectra are given and are termed molecular above threshold ionization (MATI) [11]. From figure 2 we

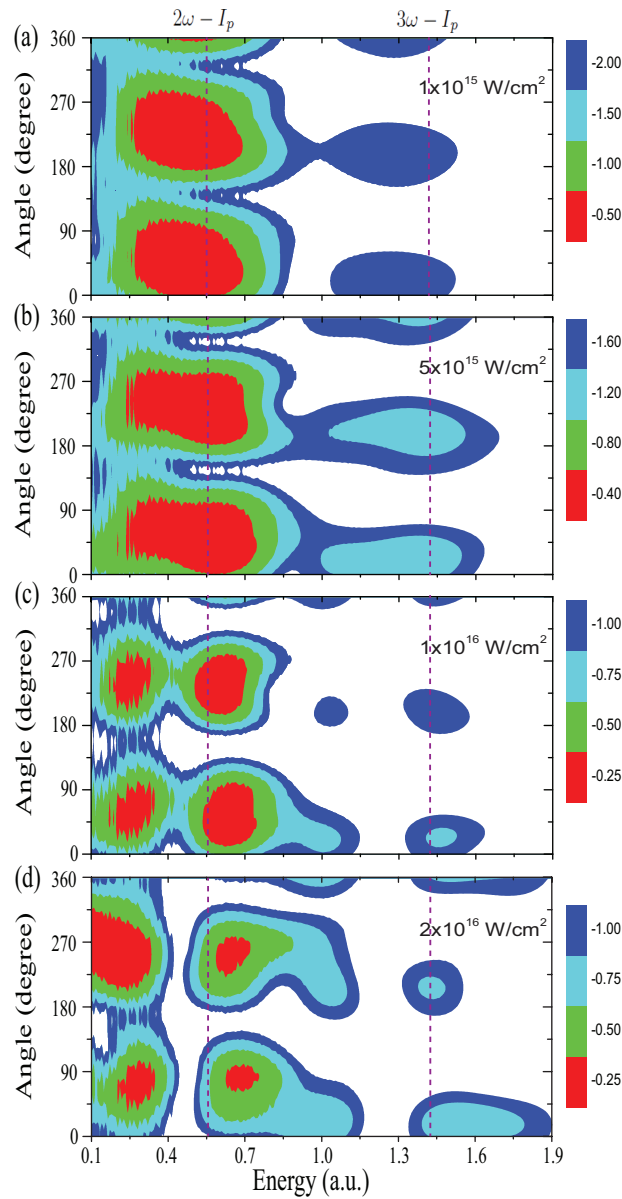


Figure 2. MPADs in H_2^+ with intense circularly polarized attosecond XUV laser pulses at $\lambda = 55 \text{ nm}$ ($\omega = 0.828 \text{ a.u.}$), FWHM=460 asec, and (a) $I = 1 \times 10^{15} \text{ W/cm}^2$ ($E = 0.169 \text{ a.u.}$), (b) $5 \times 10^{15} \text{ W/cm}^2$ (0.377 a.u.), (c) $1 \times 10^{16} \text{ W/cm}^2$ (0.534 a.u.), (d) $2 \times 10^{16} \text{ W/cm}^2$ (0.755 a.u.). Dotted lines present the classical kinetic energies $E_{en} = n\omega - I_p$ of photoelectrons.

see that the MPADs are critically sensitive to intensities of the attosecond XUV laser pulses. In figure 2(a) at the lower laser intensity $I = 1 \times 10^{15} \text{ W/cm}^2$, MPADs with peaks at kinetic energies about $E_e = 0.5 \text{ a.u.}$ and 1.3 a.u. are observed, corresponding to direct two photon ($2\omega - I_p$) and three photon ($3\omega - I_p$) ionizations. Higher order ATI peaks can also be observed in XUV laser fields and spectrum intensities decrease gradually as photoelectron kinetic energy increases [11, 12]. As the pulse intensity increases, the MPAD spectrum peaks become broad. At the pulse intensity $I = 1 \times 10^{16} \text{ W/cm}^2$ in figure 2(c), the two ATI peaks in figure 2(a) split into two separated sub-peaks with equal energy spacing $\Delta E_{AT} = 0.3 \text{ a.u.}$. It is argued here that such doublets are in fact the AT splitting which comes from the Rabi oscillation between

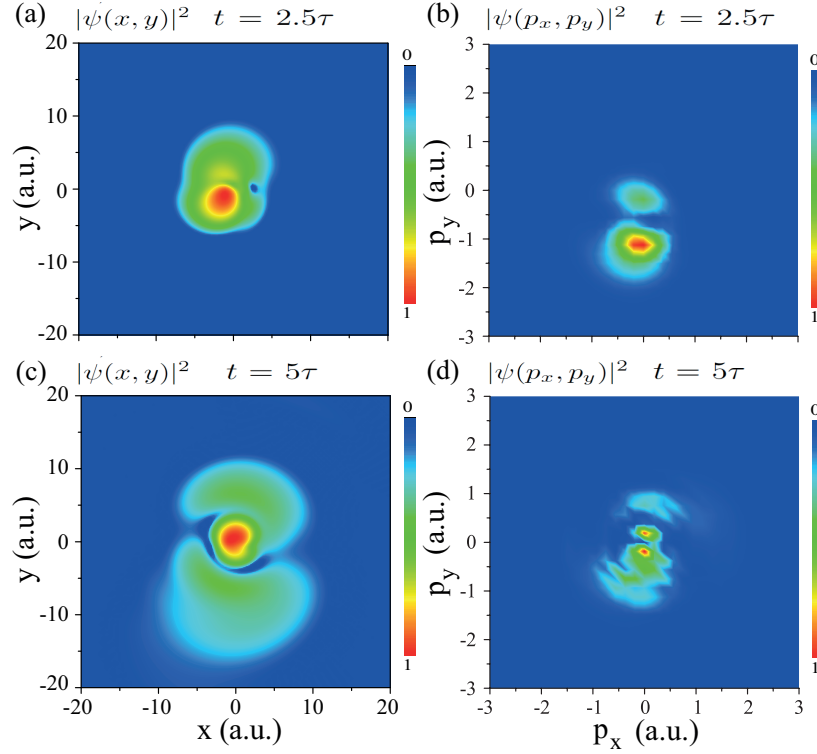


Figure 3. (Color online) Distributions of circular CEWPs, $|\psi(x, y)|^2$ and $|\psi(p_x, p_y)|^2$, in (a,c; left column) coordinate and (b,d; right column) momentum space at (a,b; upper row) $t = 2.5\tau = 460$ asec and (c,d; bottom row) $5\tau = 920$ asec with $I = 1 \times 10^{16}$ W/cm², $\lambda = 55$ nm, and FWHM=460 asec circularly polarized XUV laser pulses, cf. figure 2(c).

the ground $X^2\Sigma_g^+$ and the coherent circular Rydberg states, i.e., the excited spatially localized CEWP. Increasing the pulse intensity further to $I = 2 \times 10^{16}$ W/cm² in figure 2(d) doublets with energy spacing 0.32 a.u. are also produced. Furthermore, we emphasize that MPADs occur nearly perpendicular to the molecular internuclear x axis, i.e., near 90° and 270° instead of 0° and 180° , a feature pointed out early by Corkum and coworkers for atoms [39].

The attosecond laser pulse has FWHM=460 asec, which has a spectral width at half maximum of about $\Delta\omega = 0.3$ a.u.. Assuming the excited states are dense enough with energy spacing much less than 0.3 a.u. [figure 2(c)], a well localized electronic wave packet can be expected to be produced from the excitation of multiple Rydberg states. Figure 3 shows distributions of the CEWPs, excited by the circularly polarized attosecond XUV laser pulses at $I = 1 \times 10^{16}$ W/cm², corresponding to figure 2(c). At $t = 2.5\tau = 460$ asec, the electric field has an extremum (figure 1(b)), i.e., in the x direction and is zero in the y direction. From the electromagnetic relation $E = -\partial A/\partial t$, then $A_x = 0$ whereas A_y is maximum. Furthermore since $p(t) = -\int E(t')dt' = A(t)$ and $A_y(t) < 0$ at $t = 2.5\tau$, one sees $p_y < 0$ and $p_x = 0$, from figure 1(b), thus confirming the dominant effect of the laser field. In figure 3(a,b) the 3D plot of the circularly polarized attosecond CEWP at time $t=2.5\tau$ is spatially well confined. The circular polarization of the laser pulse enables many more Rydberg states to be excited coherently as compared to linear polarization (see below). The spatial localization of the excited circular electronic wave packet enhances the Rabi oscillation between the ground $X^2\Sigma_g^+$ and the circular coherent Rydberg states, thus leading to AT splitting in the energy spectra. At the end of the pulse ($t=5\tau=920$ asec), the circularly polarized attosecond CEWPs in the Rydberg states spread

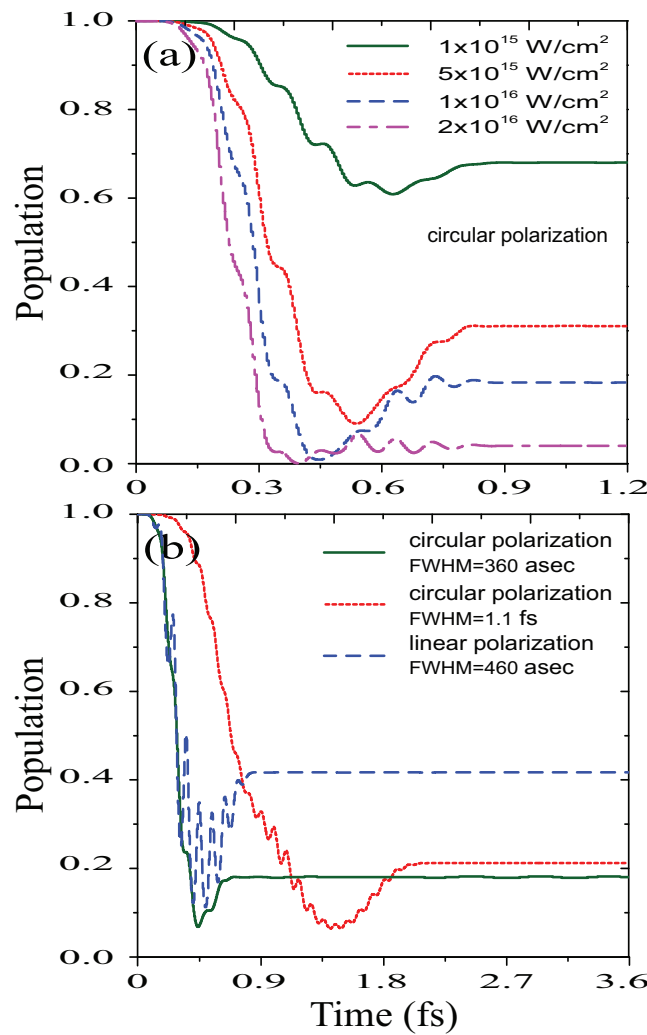


Figure 4. Population with time in the H_2^+ ground $X^2\Sigma_g^+$ state with $\lambda = 55 \text{ nm}$ attosecond XUV laser pulses. (a) FWHM=460 asec and $I = 1 \times 10^{15} \text{ W/cm}^2$ (solid line), $5 \times 10^{15} \text{ W/cm}^2$ (dotted line), $1 \times 10^{16} \text{ W/cm}^2$ (dashed line), and $2 \times 10^{16} \text{ W/cm}^2$ (dashed-dotted line) for circular polarization, cf. figure 2. (b) $I = 1 \times 10^{16} \text{ W/cm}^2$ and FWHM=360 asec (solid line) and 1.1 fs (dotted line) for circular polarization, and $I = 2 \times 10^{16} \text{ W/cm}^2$ and FWHM=460 asec (dashed line) for linear polarization, cf. figure 5.

and delocalize as illustrated in figure 3(c,d), as their radius increases with time [22].

In figure 4(a) we show evolutions of population in the ground $X^2\Sigma_g^+$ state at the four pulse intensities used in figure 2. Comparing to the weaker intensities $I = 1 \times 10^{15} \text{ W/cm}^2$ and $5 \times 10^{15} \text{ W/cm}^2$ where there is weak population transfer out of the ground state, population first decreases completely to zero, and then increases to a fixed low value for the higher laser pulse intensity $I = 1 \times 10^{16} \text{ W/cm}^2$. At $I = 2 \times 10^{16} \text{ W/cm}^2$, complete ionization occurs. Thus partial Rabi oscillations occur for intensities $I \leq 1 \times 10^{16} \text{ W/cm}^2$ between the ground $X^2\Sigma_g^+$ and the coherent Rydberg states which results in AT splitting in MPADs, as shown in figure 2(c). For photoionization at low intensities, Rabi oscillations are too slow to induce the AT splitting in the photoelectron energy spectra, as shown in figures 2(a,b). After the laser pulse switch off at time $t=920 \text{ asec}$, most of the excited electron wave packets emit, leading to

a partial constant population in the ground state. As a result, a complete Rabi oscillation does not emerge, leading to a half oscillation only, as illustrated in figure 4(a). The energy spacings between the two sub-peaks displayed in figure 2(c) defines the Rabi frequency $\Omega = \mu E$, where μ is transition dipole [30]. In figure 2(c) at intensity $I = 1 \times 10^{16}$ W/cm², the energy spacing of the AT splitting doublets is 0.3 a.u.. Therefore the average transition dipole moment between the ground $X^2\Sigma_g^+$ state and the Rydberg states can be predicted as $\mu = \Omega/E_c = \Omega/\sqrt{2}E = 0.4$ a.u.. From figure 3 we see that that period of the Rabi oscillation is about $T_{rabi} = 600$ asec, slightly longer than the prediction from the Rabi frequency $2\pi/\Omega = 503$ asec. This difference mainly results from the increasing radius of the electron wave packet in the Rydberg states, as shown in figure 3. Moreover due to ionization only a partial Rabi oscillation is produced. At larger pulse intensities, ionization occurs at an early time, thus competing with Rabi oscillations. In figure 4(a) at $I = 2 \times 10^{16}$ W/cm² most of the electron is ionized before the pulse reaches its peak intensity. Rabi oscillations are partially suppressed and a larger energy distribution in the MPADs is obtained as illustrated in figure 2(d) corresponding to larger Rabi energy splitting.

We also consider the effect of duration of the attosecond XUV laser pulses on the splitting in the energy spectra. Figure 5(a,b) shows MPADs with shorter and longer duration attosecond laser pulses at $I = 1 \times 10^{16}$ W/cm² and $\lambda = 55$ nm. The corresponding population evolutions in the H_2^+ ground $X^2\Sigma_g^+$ state are shown in figure 4(b). We see that in figure 5 the doublets in the MPAD peaks observed in figure 2(c) nearly vanish. For the shorter FWHM=360 asec photoionization in figure 5(a), the field-molecule interaction time is very short thus Rabi oscillations can not complete their cycle, as shown in figure 4(b) (black solid line). As a result, splitting in MPADs cannot be observed. Moreover, the shorter pulse spectral width is also very broad, resulting in broad photoelectron energy spectra and unresolved peaks. For longer FWHM=1.1 fs laser pulses, in figure 5(b) we see that the AT doublets are nearly absent as well. The MPAD peaks consist of two strongly asymmetric sub-peaks, one dominant and another weaker. Under such conditions, the coherent excited electron wave packets in the Rydberg states spread and delocalize during laser excitation processes, thus suppressing Rabi oscillations.

The laser polarization also plays an essential role in the CEWP generation and the AT splitting. Figure 5(c) shows the MPAD obtained with a parallel *linear* x polarization attosecond XUV laser pulse at FWHM=460 asec, $I = 2 \times 10^{16}$ W/cm² ($E_L = E_c = \sqrt{2}E$), and $\lambda = 55$ nm. We see that strongly asymmetric split doublets are obtained in the energy spectra, similar to those with a circularly polarized laser pulse at FWHM=1.1 fs in figure 5(b). For linear polarization, the electron wave packets move away from the spatial resonance region quickly. A spatially localized attosecond electron wave packet cannot be efficiently produced, in contrast to the circular polarization results illustrated in figure 3(a,b). Thus Rabi oscillations are suppressed, as shown in figure 4(b) (dashed line). Therefore, MPADs exhibit strongly asymmetric splitting as shown in figure 5(c). Comparing to the results of circular polarization photoionization in figures 4(a) and 4(b), population of the ground electronic state in figure 4(b) (blue dashed line) exhibits a strong sub-oscillation from about 200 asec to 800 asec, corresponding to the driving pulse duration. This oscillation mainly results from the recollision of the free electron, following the classical three-step model [40]. Moreover one sees clearly that more angle nodes are observed in the two- and three-photon MATI peaks, which disappear with higher order ionization. This is mainly due to scattering effects of ejected electrons in photoionization processes [41].

We note furthermore that, in the MPADs with circularly polarized attosecond XUV laser pulses in figures 2 and 5(a,b), the photoionization distributions are mainly localized along the y polarization ($\theta = 90^\circ$ and 270°) perpendicular to the molecular x -axis, as compared to MPADs parallel to the molecular x axis for linear polarization. This mainly results from the effects of the electronic charge clouds associated with each scattering center in the photoelectron ionization processes, leading to orientation-dependent ionization rates, which allows for tomographic imaging of molecular orbitals [34, 42]. Moreover, the MPAD is seen to be rotated with respect to

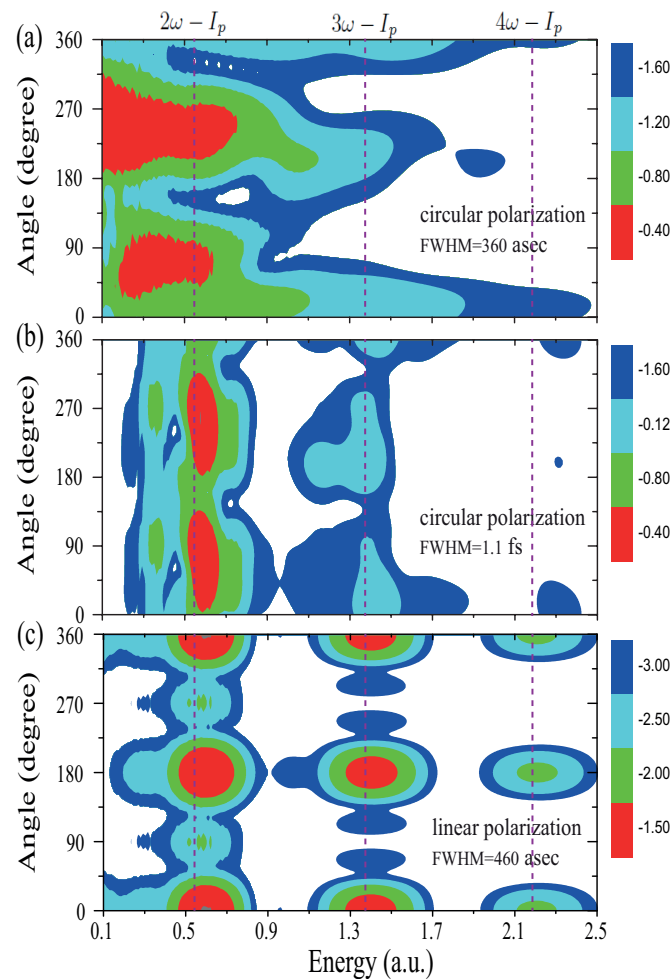


Figure 5. MPADs in H_2^+ with wavelength $\lambda = 55$ nm, (a,b) circularly and (c) linearly polarized attosecond XUV laser pulses. The other laser parameters are (a) FWHM= 360 asec and intensity $I = 1 \times 10^{16}$ W/cm², (b) FWHM=1.1 fs and intensity $I = 1 \times 10^{16}$ W/cm², and (c) FWHM= 460 asec and intensity $I = 2 \times 10^{16}$ W/cm². Dotted lines present the classical kinetic energies $E_{en} = n\omega - I_p$ of photoelectrons.

the laser perpendicular y polarization axis due to the two center nonspherical Coulomb potential as well. Both orientation-dependent ionization rates and rotation angles of MPAD of aligned H_2^+ are shown to be sensitive to the photoelectron energies [32, 43, 44].

Of note is that in the photoelectron energy spectra illustrated in figures 2 and 5, MATI peaks exhibit a signature of energy shifts to low energy region relative to the classical kinetic energies $E_{en} = n\omega - I_p$ (dashed lines). This mainly results from the broad spectral width of the attosecond pulse since the photoelectron distributions are functions of the pulse spectral width and the Franck-Condon factor between the initial ground and the continuum electronic states. The energy shift has also been observed in the attosecond photoionization processes of H and He atoms with linearly polarized ultrashort few cycle XUV laser pulses [45, 46].

4. Conclusions

In summary, AT doublets in circular polarization MPADs of H_2^+ have been reported from circular CEWPs. These are excited by a circularly polarized attosecond XUV laser pulse at FWHM=460

asec and $\lambda = 55$ nm. An energy splitting of the AT-MPAD spectra is observed as a result of partial Rabi oscillations between spatially localized circular electron wave packets and the initial ground electronic state. Results from numerical solutions of appropriate TDSEs show that the circularly polarized attosecond CEWPs of Rydberg states created by a circularly polarized laser pulse with proper duration, intensity and wavelength is required to produce Rabi frequency and then to observe such splitting in energy spectra. The essence of the attosecond AT doublets is to induce spatially localized circular polarization CEWPs in the photoionization processes. Moreover, rotations of the angular distribution of the energy-resolved photoelectron with respect to the laser polarizations is observed as well, reflecting the influence of the nonspherical Coulomb potential in the molecule.

Acknowledgements

We thank RQCHP and Compute Canada for access to massively parallel computer clusters and NSERC for financial support in ultrafast science program. ZGS is supported by the National Natural Science Foundation of China (Grant No. 21222308, 2013CB922202, 21133006), the Chinese Academy of Sciences, and Ministry of Science and Technology of China.

References

- [1] Krausz F and Ivanov M 2009 *Rev. Mod. Phys.* **81** 163
- [2] Chang Z and Corkum P 2010 *J. Opt. Am. B* **27** B9
- [3] Chelkowski S, Yudin G L and Bandrauk A D 2006 *J. Phys. B* **39** S409
- [4] Niikura H, Villeneuve D M and Corkum P B 2005 *Phys. Rev. Lett.* **94** 083003
- [5] Shao H C and Starace A F 2010 *Phys. Rev. Lett.* **105** 263201
- [6] Kelkensberg F, Rouzée A, Siu W, Gademann G, Johnsson P, Lucchini M, Lucchese R R and Vrakking M J J 2011 *Phys. Rev. A* **84** 051404(R)
- [7] Mauritsson J, Remetter T, Swoboda M, Klünder K, L'Huillier A, Schafer K J, Ghafur O, Kelkensberg F, Siu W, Johnsson P, Vrakking M J J, Znakovskaya I, Uphues T, Zharebtsov S, Kling M F, Lépine F, Benedetti E, Ferrari F, Sansone G and Nisoli M 2010 *Phys. Rev. Lett.* **105** 053001
- [8] Ranitovic P, Tong X M, Hogle C W, Zhou X, Liu Y, Toshima N, Murnane M M and Kapteyn H C 2011 *Phys. Rev. Lett.* **106** 193008
- [9] Choi N N, Jiang T F, Morishita T, Lee M H and Lin C D 2010 *Phys. Rev. A* **82** 013409
- [10] Baggesen J C and Madsen L B 2011 *Phys. Rev. A* **83** 021403(R)
- [11] Yuan K J and Bandrauk A D 2012 *Phys. Rev. A* **85** 013413
- [12] Yuan K J, Lu H Z and Bandrauk A D 2013 *ChemPhysChem* **14** 1496
- [13] Feist J, Nagele S, Pazourek R, Persson E, Schneider B I, Collins L A and Burgdörfer J 2009 *Phys. Rev. Lett.* **103** 063002
- [14] Moore L R, Lysaght M A, Parker J S, van der Hart H W and Taylor K T 2011 *Phys. Rev. A* **84** 061404(R)
- [15] Jiang Y H, Rudenko A, Herrwerth O, Foucar L, Kurka M, Kühnel K U, Lezius M, Kling M F, van Tilborg J, Belkacem A, Ueda K, Dusterer S, Treusch R, Schröter C D, Moshhammer R and Ullrich J 2010 *Phys. Rev. Lett.* **105** 263002
- [16] Demekhin P V and Cederbaum L S 2012 *Phys. Rev. Lett.* **108** 253001
- [17] Wang X and Eberly J H 2009 *Phys. Rev. Lett.* **103** 103007
- [18] Wang X and Eberly J H 2010 *Phys. Rev. Lett.* **105** 083001
- [19] Mauger F, Chandre C and Uzer T 2010 *Phys. Rev. Lett.* **104** 043005
- [20] Mauger F, Chandre C and Uzer T 2010 *Phys. Rev. Lett.* **105**, 083002
- [21] Ceccherini F, Bauer D and Cornolti F 2003 *Phys. Rev. A* **68** 053402
- [22] Yuan K J and Bandrauk A D 2012 *J. Phys. B* **45** 074001
- [23] Yuan K J and Bandrauk A D 2013 *Phys. Rev. Lett.* **110** 023003
- [24] Barth I, Manz J, Shigeta Y and Yagi K 2006 *J. Am. Chem. Soc.* **128** 7043
- [25] Barth I and Manz J 2007 *Phys. Rev. A* **75** 012510
- [26] Bauer D and Ceccherini F 2002 *Phys. Rev. A* **66** 053411
- [27] Yuan K J and Bandrauk A D 2013 *Phys. Rev. A* **88** 013417
- [28] Autler S H and Townes C H 1955 *Phys. Rev.* **100** 703
- [29] Palacios A, Bachau H and Martín, F 2006 *Phys. Rev. A* **74** 031402(R)
- [30] Sun Z and Lou N 2003 *Phys. Rev. Lett.* **91** 023002
- [31] Yuan K J, Sun Z, Cong S L and Lou N 2006 *Phys. Rev. A* **74** 043421

- [32] Yuan K J and Bandrauk A D 2012 *Phys. Rev. A* **85** 053419
- [33] Yuan K J and Bandrauk A D 2012 *J. Phys. B* **45** 105601
- [34] Kamta G L and Bandrauk A D 2005 *Phys. Rev. A* **71** 053407
- [35] Kamta G L and Bandrauk A D 2006 *Phys. Rev. A* **74** 033415
- [36] Lee K F, Villeneuve D M, Corkum P B, Stolow A and Underwood J G 2006 *Phys. Rev. Lett.* **97** 173001
- [37] Bandrauk A D and Shen H 1993 *J. Chem. Phys.* **99** 1185
- [38] Bandrauk A D and Lu H Z 200 *High-Dimensional Partial Differential Equations in Science and Engineering*, edited by Bandrauk A D, Delfour M and LeBris C, CRM Lecture Series Vol. 41 American Math. Soc. Philadelphia 1-15
- [39] Corkum P B, Burnett N H and Brunel F 1989 *Phys. Rev. Lett.* **62** 1259
- [40] Corkum P B 1993 *Phys. Rev. Lett.* **71** 1994
- [41] Bauch S and Bonitz M 2008 *Phys. Rev. A* **78** 043403
- [42] Meckel M, Comtois D, Zeidler D, Staudte A, Pavicic D, Bandulet H C, Pépin H, Kieffer J C, Dörner R, Villeneuve D M and Corkum P B 2008 *Science* **320** 1478
- [43] Yuan K J, Chelkowski S and Bandrauk A D 2013 *J. Chem. Phys.* **138** 134316
- [44] Yuan K J, Chelkowski S and Bandrauk A D 2014 *Chem. Phys. Lett.* **592** 334
- [45] Peng L Y and Starace A F 2007 *Phys. Rev. A* **76** 043401
- [46] Peng L Y, Pronin E A and Starace A F 2008 *New J. Phys.* **10** 025030